Transactions of the Materials Research Society of Japan 28 [3] 879-882 (2003)

Nanoparticle Formation by Pulsed Laser Ablation of TiO_2

Tetsuya Yamaki, Hisayoshi Itoh, Masakazu Matsubara*, Hiroaki Abe** and Keisuke Asai*
Department of Material Development, Takasaki Radiation Chemistry Research Establishment,
Japan Atomic Energy Research Institute, 1233 Watanuki, Takasaki, Gunma 370-1292, Japan
Fax: 81-27-346-9687, e-mail: tetsuya@taka.jaeri.go.jp
*Department of Quantum Engineering and Systems Science, Graduate School of Engineering, The University of Tokyo,
7-3-1 Hongo, Bunkyo-ku, Tokyo 113-8656, Japan
**Nuclear Engineering Research Laboratory, Graduate School of Engineering, The University of Tokyo,
2-22 Shirakata-Shirane, Tokai-mura, Naka-gun, Ibaraki 319-1188, Japan

Nanoparticle formation by pulsed laser ablation of a titanium dioxide (TiO_2) pellet with a KrF excimer laser (λ = 248 nm) was investigated. The ablation in an atmosphere of Ar and O_2 (5:5) at total pressures of □ 1 Torr led to the formation of TiO_2 particles composed of anatase and rutile structures without any suboxides. The relative content of the rutile phase in such phase-mixed nanoparticles was controlled by the Ar/O_2 ambient pressure; the content became large as the pressure increased from 1 to 10 Torr. No shift in the bandgap energy was observed for the TiO_2 particles, indicating that no quantum size effects occurred. From transmission electron microscopy observations, the particle size was found to range from 10 and 14 nm, which far exceeded the previously calculated exciton radius of 0.75-1.9 nm.
Key words: titanium dioxide (TiO_2), nanoparticles, pulsed laser ablation, laser plasma, quantum size effect

1. INTRODUCTION

Titanium dioxide (TiO_2) fine particles have received much attention because they exhibit pronounced size effects on their electronic and optical properties. For example, the photocatalytic activity of TiO_2 particles increased when their diameter became smaller than about 10 nm [1]. According to the crystallographic classification, TiO_2 is known to have two main tetragonal structures, anatase and rutile. Rutile is a high-temperature, stable phase, and anatase is a low-temperature, metastable polymorph. Generally, anatase has more active photoelectrochemical properties than rutile. Fotou et al. [2], however, reported that the photoactivity of anatase TiO_2 *mixed with the rutile phase* was higher than that of pure anatase for the decomposition reaction of phenol. Degussa P25, a commercial powder material frequently used in photocatalysis studies, contains both the rutile and anatase phases in the appropriate proportions. The observation of the relatively high photoactivity for this form of TiO_2 was interpreted in terms of the enhancement of the magnitude of the space-charge potential, which is created by contact between the different phases [3]. The fabrication of TiO_2 nanoparticles containing such mixed phases, therefore, is of paramount importance.

Among the many routes for producing metallic or nonmetallic nanoparticles, pulsed laser ablation (PLA) [4-6] has been developed as a promising gas-phase method because of the following advantages: (i) The chemical contamination of particles is suppressed because it is a high-vacuum technique. (ii) High power lasers evaporate materials with a high boiling point, even metal oxides. This allows versatility in preparing many kinds of particles, and (iii) The most important one is that the ablation conditions are easily controlled by many variables such as the wavelength and fluence of the laser, and the type and pressure of the ambient gas. In a previous study, ultrasmall TiO_2 particles were prepared by the PLA of a rutile target rod [7]. However, these nanoparticles were found to consist of only the anatase phase since the ablation conditions were not significantly varied.

In the present study, we prepared TiO_2 nanoparticles with the crystalline phases of rutile and anatase by the PLA technique and then investigated their stoichiometry, crystal structure, electronic property and size. Importantly, the rutile/anatase ratio in the particles was controlled by changing the conditions of the laser ablation, especially the ambient gas pressure.

2. EXPERIMENTAL

Figure 1 shows the experimental apparatus consisting of a laser radiation system (Lambda Physik 105icc) and a vacuum deposition chamber. Particles were deposited on an α-Al_2O_3 (0001) substrate by irradiating a sintered pellet of high-purity rutile TiO_2 (99.99%) with a KrF excimer laser (λ = 248 nm) in an Ar/O_2 gas mixture (5:5). The incident angle of the laser beam on the target was 45°. The repetition rate and fluence of the laser were 10 Hz and 6.3 J/cm^2, respectively. In the chamber, the substrate was maintained at room temperature and placed under the laser plume so as not to contact each other (see (b)). The pressures of the Ar/O_2 ambient gas were varied from 0.2 to 10 Torr.

X-ray photoelectron spectroscopy (XPS) using Mg Kα (hν = 1253.6 eV) radiation gave information regarding the chemical states of the elements in the obtained nanoparticles. The crystal structures were determined by X-ray diffraction (XRD) with Cu Kα radiation (λ = 0.1542

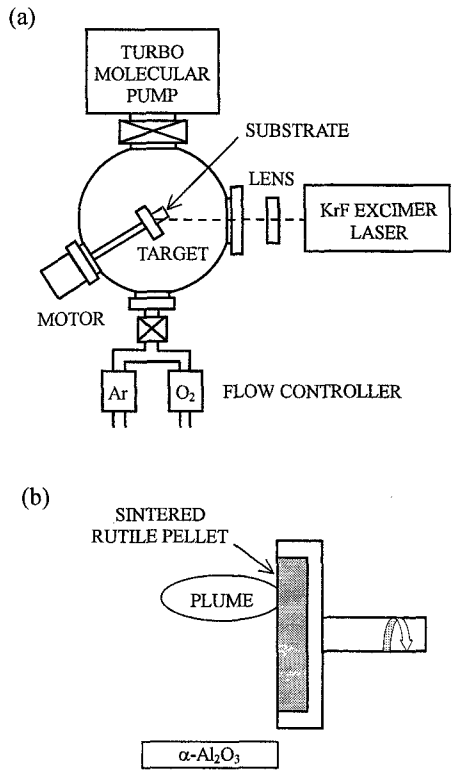

Fig. 1. Schematic diagram of the PLA apparatus for nanoparticle formation. (b) shows target and substrate configurations during the ablation.

nm) through a Ni filter. UV-vis absorption measurements were made in a colloidal dispersion of 2-propanol at room temperature. The size and shape were characterized using a transmission electron microscope (TEM) operated at 200 kV. For the TEM observations, the nanoparticles dispersed in 2-propanol were placed on a carbon-coated copper grid.

3. RESULTS AND DISCUSSION

Figure 2 shows the Ti 2p XPS spectra of the samples synthesized at pressures of 0.2 and 5 Torr. At 5 Torr, the Ti $2p_{3/2}$ and $2p_{1/2}$ levels were located at 458.3 and 464.1 eV, respectively. These binding energies and splitting of the doublet (□BE = 5.8 eV) confirm an oxidation state of 4+ for titanium, in other words, the complete oxidation to TiO_2. In contrast, at 0.2 and 0.5 Torr, the Ti 2p peaks were shifted to the lower energy region and became slightly broader, indicative of a mixture of suboxide Ti_2O_3.

Figure 3 displays the θ-2θ XRD patterns of the TiO_2 nanoparticles prepared on the α-Al_2O_3 substrate at 1 and 5 Torr. The patterns possessed several diffraction peaks, each of which corresponds to the rutile or anatase phase, in addition to a strong peak from the substrate. The vapor-phase energetic reactions undoubtedly occur in the laser plasma to generate TiO_2 crystallites with both rutile and anatase phases. On the other hand, a small amount of Ti_2O_3 was mixed with the two phases of TiO_2 in the samples prepared at 0.2 and 0.5 Torr, as evidenced by the above XPS result.

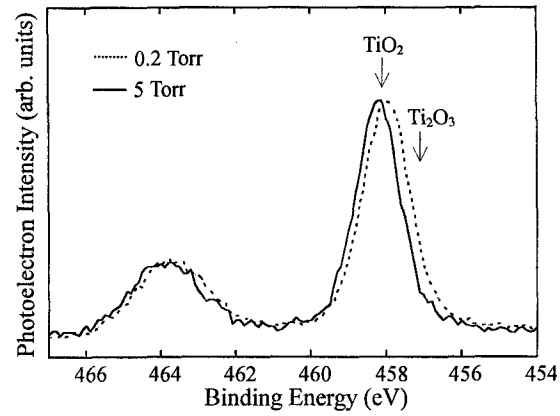

Fig. 2. Ti 2p XPS spectra of the TiO_2 nanoparticles prepared on the α-Al_2O_3 substrate at the ambient pressures of 0.2 (dashed line) and 5 Torr (solid line).

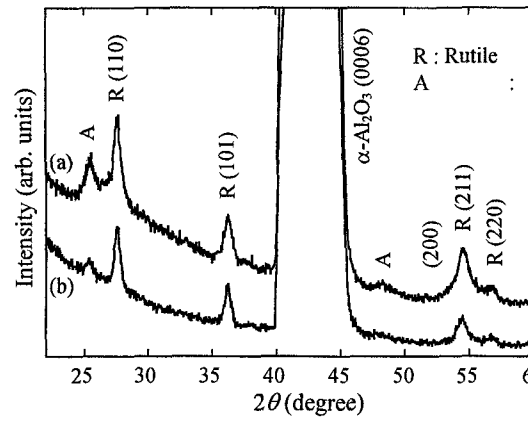

Fig. 3. θ-2θ XRD patterns of the TiO_2 nanoparticles prepared on the α-Al_2O_3 substrate at the ambient pressures of (a) 1 and (b) 5 Torr. The diffraction peaks for rutile and anatase are denoted by R and A, respectively.

It should be noted here that the relative intensities of the XRD peaks corresponding to the rutile and anatase phases were different. The weight fraction of the rutile phase present in the particles, f, is calculated by the empirical equation given below [8]:

$$f = 1 - \frac{1}{1 + 1.26\,(I_R/I_A)} \qquad (1)$$

where I_R and I_A are the integrated intensities of the (110) reflection of rutile and the (101) reflection of anatase, respectively. In Fig. 4, the weight fractions of rutile are plotted as a function of the Ar/O_2 pressure. It is apparent that the rutile-to-anatase ratio in the TiO_2 particles became significant as the background gas pressure increased from 1 to 10 Torr. Consequently, the relative content of the rutile phase was controlled between 70 and 90% by varying the ambient pressure.

Furthermore, the size of the TiO_2 crystallites, t, was calculated from the XRD data using the Scherrer formula as follows:

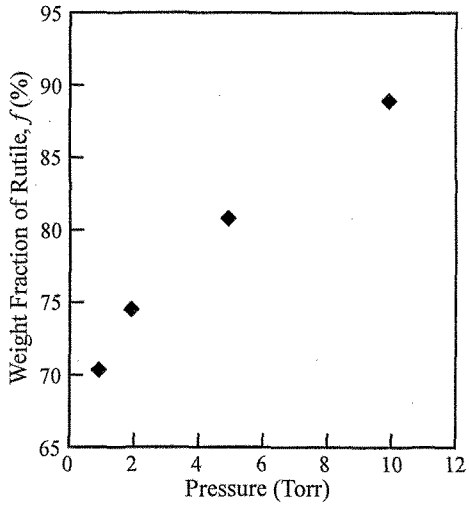

Fig. 4. Weight fraction of the rutile phase in the TiO_2 nanoparticles as a function of the ambient pressure between 1 and 10 Torr.

$$t = \frac{0.9\,\lambda}{B\cos\theta} \qquad (2)$$

where B is the full-width of the peak at half maximum and λ is the wavelength of the Cu Kα radiation. The crystalline size of the rutile phase was between 13 and 17 nm, and that of the anatase phase ranged from 12 to 15 nm. The crystalline size seemed to be independent of the gas pressure and crystal structures of TiO_2.

The phase-mixed TiO_2 nanoparticles crystallize in the plasma induced by the PLA of the rutile pellet. It is reasonable, therefore, to consider that the formation of the rutile/anatase phases is directly affected by the conditions of the laser plasma. The plasma formation using various kinds of laser sources was characterized by the optical emission measurements of a plume [9] and the Q-mass analyses of the excited species [7]. According to these previous investigations, high power lasers in the UV range, whose photon energy exceeds the bandgap of TiO_2, generated plasmas with high electronic excitations. Under this condition, TiO_2 was completely decomposed into individual atoms and ions of Ti or O, therefore, few molecular species like TiO and TiO_2 were present in the plasma.

As already shown in Fig. 4, the rutile content increased with an increase in the pressures of the mixed gas. Thus, under the higher ambient pressure, the reaction is considered to promote the formation of the rutile-phase TiO_2. In our experiment, the background gas pressures varied the density of the excited species in the plasma. S. -M. Oh et al. [10] prepared TiO_2 powders of the rutile/anatase mixed phases by the oxidation of $TiCl_4$ using a thermal plasma. Their important result is that rutile crystallized in the higher temperature region in the plasma while anatase was formed in the lower temperature region. The temperature of the plasmas rises as their density increases, as assessed by theoretical calculations based on the time-dependent collisional-radiative model for describing the population densities of the excited states [11]. In our case, therefore, an increase in the plasma density corresponds to the higher-temperature preparation of TiO_2 nanoparticles, thereby enhancing the weight fraction of rutile. Our method enables the crystalline phases of the TiO_2 nanoparticles to be controlled by changing the laser-plasma condition.

The UV-vis absorption spectra were identical to each other. Thus the contribution of the existing anatase phase to the absorption features is small enough to be ignored. This is probably because the rutile is the dominant phase and also has the larger optical absorption coefficient, α, compared to the anatase. Estimates of the bandgap energy for the TiO_2 nanoparticles were done by the absorption data. For indirect semiconductors such as TiO_2, the minimum of the lowest conduction band is shifted relative to the maximum of the highest valence band, and the lowest-energy interband transition must then be accompanied by phonon excitation. The coefficient α (calculated from the raw spectrum [12]) near the absorption edge for indirect interband transitions is given by eq. 3

$$\alpha = A_i(h\nu - E_g)^2/h\nu \qquad (3)$$

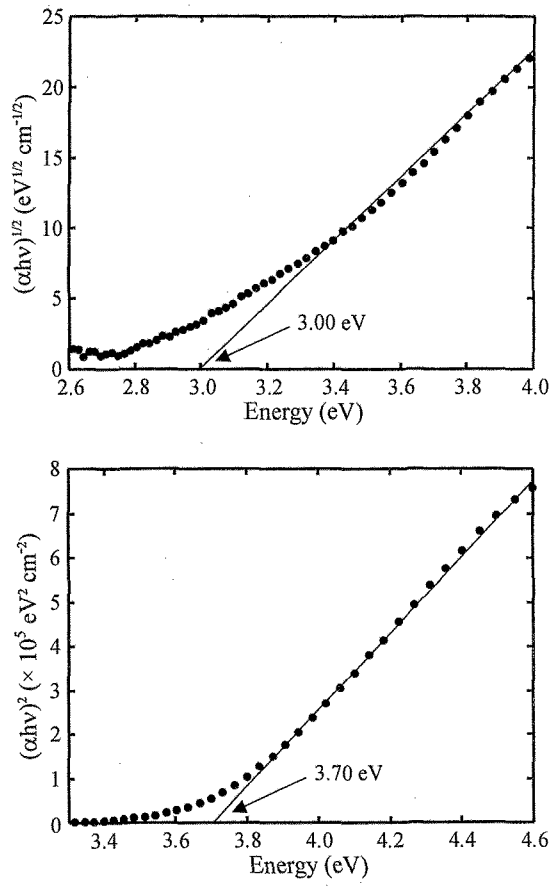

Fig. 5. (a) Plots of $(\alpha h\nu)^{1/2}$ versus photon energy for the TiO_2 nanoparticles prepared at 5 Torr. Absorption coefficients, α, were calculated from the raw spectra. (b) Plots of $(\alpha h\nu)^2$ versus photon energy for the same sample. The measurements were made in a colloidal dispersion of 2-propanol.

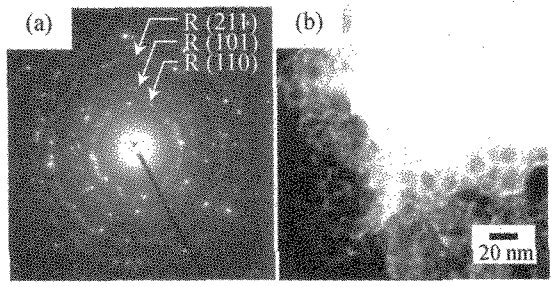

Fig. 6. Representative TEM result of the TiO_2 nanoparticles prepared at the ambient pressure of 10 Torr. The image (a) shows the electron diffraction pattern of the TiO_2 nanoparticles, together with the indices of the crystal faces corresponding to the observable fringes.

where A_i is the absorption constant for an indirect transition. Accordingly, a plot of $(\alpha h\nu)^{1/2}$ versus photon energy was obtained for the sample prepared at 5 Torr, as shown in Fig. 5 (a). This plot gave a straight line whose intercept on the horizontal axis occurs at 3.00 eV. The absorption onset is ascribed to the bandgap edge of the rutile TiO_2. Our present findings clearly show that the TiO_2 nanoparticles possessed bulk rutile bandgaps and, therefore, there is no size quantization in their size regime.

Plots of $(\alpha h\nu)^{1/2}$ versus photon energy in Fig. 5 (a) displayed no linear relationships above 3.6 eV as were expected for the lowest interband transition in the indirect semiconductor TiO_2. In contrast, linear relationships obtained only when the absorption coefficient data were plotted as $(\alpha h\nu)^2$ versus photon energy in the higher energy region (Fig. 5 (b)). The much stronger absorption features were observed due to the allowed direct band transitions in an otherwise indirect bandgap semiconductor. The extrapolation of the linear region to $(\alpha h\nu)^2 = 0$ in the plot of Fig. 5 (b) provides an estimation of the intercept at 3.70 eV, where these (direct) Franck-Condon type transitions occur [13].

It was not totally unexpected that there appeared no shift in the bandgap energy, normally associated with decreasing particle size. Semiconductor fine particles exhibit quantum size effects due to exciton confinement when their size becomes comparable to the size of the exciton. The exciton radii between 0.75 and 1.9 nm were previously computed for small TiO_2 particles by using the various literature values based on condensed-matter physics [14]. The size of our TiO_2 nanoparticles, as also shown below, was in the range of 10 nm, which far exceeds these values.

Figure 6 depicts the TEM results of the TiO_2 nanoparticles prepared in the atmosphere at 10 Torr. The electron diffraction of the nanoparticles exhibited fringe patterns corresponding to the (110), (101) and (211) crystal faces of rutile TiO_2. The diffraction fringes from the anatase phases were not observed because of their small amount. The samples were evenly distributed with a spherical shape and their average size was 10-14 nm, irrespective of the ablation conditions. Within experimental error, this value is in agreement with that estimated by the Scherrer equation.

The optical responses of TiO_2 are mainly induced under the near UV light (350-400 nm). In this sense, the increase in the TiO_2 bandgap is not advantageous for photocatalyst applications because this hinders the effective utilization of solar beams. As mentioned in the introduction, the TiO_2 powders with particle diameters as small as approximately 10 nm exhibit a greater reactivity. Our rutile/anatase mixed nanoparticles are in this size range and allow the large surface area to be provided for photocatalytic reactions without any bandgap change. Therefore, such materials can offer possibilities of future developments in the applications of TiO_2 photocatalysts.

4. CONCLUSIONS

We successfully prepared TiO_2 nanoparticles by the PLA under various Ar/O_2 gas pressures. The nanoparticles formed at pressures of 1-10 Torr contained both the rutile and anatase phases of TiO_2. The samples were spherical particles with diameters of 10-14 nm and displayed no size quantization (i.e., no shift in the bandgap energy). The PLA technique made it possible to control the rutile/anatase ratio in the TiO_2 nanoparticles by varying the ambient gas pressure.

REFERENCES

[1] M. Anpo, T. Shima, S. Kodama, and T. Kubokawa, *J. Phys. Chem.*, **91**, 4305-10 (1987).
[2] G. P. Fotou and S. Partsinis, *Chem. Eng. Commun.*, **151**, 251-69 (1996).
[3] R. I. Bickley, T. Gonzalez-Carreno, J. S. Lees, L. Palmisano, and R. J. D. Tilley, *J. Solid State Chem.*, **92**, 178-90 (1991).
[4] T. Yoshida, S. Takeyama, Y. Yamada, and K. Mutoh, *Appl. Phys. Lett.*, **68**, 1772-74 (1996).
[5] J. S. Jeon and C. S. Yeh, *J. Chin. Chem. Soc.*, **45**, 721-26 (1998).
[6] Q. Li, T. Sasaki, and N. Koshizaki, *Appl. Phys. A*, **69**, 115-18 (1999).
[7] K. Kawasaki, J. F. Despres, S. Kamei, M. Ishikawa, and O. Odawara, *J. Mater. Chem.*, 7, 2117-20 (1997).
[8] R. A. Spurr and H. Myers, *Anal. Chem.*, **29**, 760-62 (1957).
[9] A. De Giacomo, V. A. Shakhatov, and O. De Pascale, *Spectrochim. Acta B*, **56**, 753-76 (2001).
[10] S. -M. Oh, J. -G. Gong, and D. -W. Park, *J. Chem. Eng. Jpn.*, **34**, 283-86 (2001).
[11] M. Capitelli, F. Capitelli, and A. Eletskii, *Spectrochim. Acta B*, **55**, 559-74 (2000).
[12] W. N. Delgass, G. L. Haller, R. Kellerman, and J. H. Lunsford, "Spectroscopy in Heterogeneous Catalysis", Academic Press, New York (1979) p. 128.
[13] N. Serpone, D. Lawless, and R. Khairrutdinov, *J. Phys. Chem.*, **99**, 16646-54 (1995).
[14] C. Kormann, D. W. Bahnemann, and M. R. Hoffmann, *J. Phys. Chem.*, **92**, 5196-5201 (1988)

(Received December 20, 2002; Accepted March 1, 2003)